A Compact L-Band Orthomode Transducer for Radio Astronomical Receivers at Cryogenic Temperature

Giuseppe Valente, Giorgio Montisci, *Member, IEEE*, Tonino Pisanu, Alessandro Navarrini, and Giovanni A. Casula, *Member, IEEE*

***Abstract*—We describe the design, construction and performance of a compact orthomode transducer (OMT) for the L-band receiver (1.3 GHz - 1.8 GHz) of the Sardinia Radio Telescope (SRT). The complete OMT consists of a cylindrical orthomode junction (OMJ), which is presented in this paper, and two identical 180° hybrid power combiners in double ridged waveguide, which have been proposed in a previous work. The OMT operates at the cryogenic temperature of 20 K to reduce its thermal noise contribution to the noise of the receiving chain. Therefore, particular care has been taken in the design of the OMJ to minimize its dimension and insure a good thermalization. The proposed OMT has been designed and optimized by using CST Microwave studio, and then manufactured, tested at room temperature, and installed on the L-band receiver of SRT. The measured results fully comply with the design specifications. In particular, the isolation between the OMT output ports is more than 40 dB, and the cross polarization is less than -35 dB for both polarization channels.**

***Index Terms*— Cryogenics, L-band, Orthomode Transducer, Radio astronomy, Sardinia Radio Telescope**

I. Introduction

ORTHOMODE Transducers (OMTs) are key components of dual-polarized antenna feed systems and allow splitting two orthogonal linearly polarized signals within the same frequency band. An OMT is a passive microwave component that has three physical ports but exhibits properties of a four-port device, because the input common port, usually a waveguide with a square or a circular cross-section, provides two electrical ports that correspond to the two independent orthogonal polarized signals [1].

The requirements of OMTs used in modern radio astronomy applications are high cross-polarization discrimination between orthogonal signals, typically below -35 dB, and good input match of all electrical ports over a relative frequency bandwidth prescribed by radio astronomy constraints, typically of order 30-40% for high-performance waveguide-based structures.

Aim of this paper is to develop a compact OMT to be used in the L-Band receiver of the Sardinia Radio Telescope (SRT) [2], a new, general purpose, fully steerable 64 m diameter parabolic radio telescope capable to operate with high efficiency over the 0.3-116 GHz frequency range.

The operating frequency range of the L-Band receiver of SRT has been selected between 1.3 GHz - 1.8 GHz to achieve the widest radio astronomy performance, while avoiding adjacent-channel interference. In particular, the main radio astronomy targets of the L-Band receiver of SRT are pulsar observation, HI-line (1420 MHz) and OH-line (1600 MHz, 1612 MHz, 1667 MHz and 1720 MHz) studies, and VLBI (Very Long Baseline Interferometry) observations (in the frequency bands 1350 MHz -1450 MHz and 1625 MHz -1715 MHz).

In order to reduce the system noise temperature of the L-Band receiver chain, some of the key components (OMT, directional couplers [3], and Low Noise Amplifiers) are thermalized at cryogenic temperatures and housed inside a compact cryostat. The cryogenic system consists of a two-stage cryo-cooler with nominal temperatures of 20 K and 77 K. The design of the cryostat is constrained by the limited space available in the direction of the optical axis inside the focal cabin of the radio telescope, thus requiring a very compact design of all components of the receiver chain, including the OMT.

The most popular OMTs employed in radio astronomy are based on the Bøifot configuration [4] and on the turnstile junction configuration [5-8]. Both of these solutions allow to achieve a large frequency bandwidth, which is necessary in radio astronomy receivers. However, the Bøifot and turnstile junction OMT configurations are not suitable for scaling at low frequencies because large size structures would be required. Thus, alternative solutions have been studied (see e.g. [9-19]). In [9] a L-Band compact Orthomode Junction (OMJ) was proposed, based on four single-ridged triangular waveguides. The total dimension of this OMJ is 2.24 λ_0 × 0.66 λ_0 × 0.66 λ_0. However, in that paper, no details are available on the architecture and dimension of the 180° hybrids used to recombine the out-of-phase signals at the four outputs of the OMJ. In [10] a L-Band OMT, based on a quad-ridged waveguide, is presented. In this case, the total length of the

Manuscript received January 5, 2015.

Giuseppe Valente, Tonino Pisanu and Alessandro Navarrini are with INAF - Osservatorio Astronomico di Cagliari, Via della Scienza 09047 Selargius, Italy. (e-mail: valente@oa-cagliari.inaf.it, tpisanu@oa-cagliari.inaf.it, navarrin@oa-cagliari.inaf.it).

Giorgio Montisci and Giovanni A. Casula are with Dipartimento di Ingegneria Elettrica ed Elettronica, Università degli Studi di Cagliari, 09123 Cagliari, Italy (e-mail: giorgiom@diee.unica.it, a.casula@diee.unica.it).

component is 3.4 λ_0. Therefore, both configuration of [9] and [10] are quite large and then unsuitable to be housed inside the compact cryostat used for SRT.

In [11] a K-band orthomode transducer is proposed, consisting of orthogonal balanced coaxial probes in a circular waveguide, linked by coaxial transmission lines to balanced coaxial probes in orthogonal WR42 waveguides. Unfortunately, a simple rescaling of that configuration at the frequencies of our interest (i.e. in the L-Band) would also lead to a cumbersome structure which could not be arranged inside a compact cryostat.

Other OMT configurations based on circular (or rectangular) waveguides and using planar probes to extract the orthogonal polarizations, have been proposed in [12-16]. However, all these solutions were not intended to operate at cryogenic temperature, and, clearly, no suggestion is given on how performing the required thermal isolation between the room temperature and cryogenic temperatures.

A compact OMT configuration, suitable for operation at the cryogenic temperature of 77 K, was proposed by Lehmensiek and Theron [17-19]. That OMT design is based on two orthogonal dipoles placed in a circular waveguide and on two Marchand baluns that convert the balanced transmission lines from the dipoles into unbalanced coaxial transmission lines.

In this paper we present a L-Band OMT, which is intended to operate at the temperature of 20 K, with a significant reduction of the system noise temperature compared to the solution presented in [17-19], which employs an OMT designed to operate at the higher temperature of 77 K. Moreover, in the receiver of the MeerKAT system [19], the OMT and the directional coupler operate at 77 K, whereas the LNA operates at 20 K, and a connection cable for thermal isolation between the directional coupler and the LNA is necessary. This cable adds a further noise contribution between 1 K and 1.5 K in the receiver chain of the MeerKAT system [19]. On the other hand, in our case, the OMT, the directional coupler, and the LNA are all refrigerated at the same cryogenic temperature of 20 K, thus no cable providing thermal isolation is required between the directional coupler and the LNA. As a consequence, lowering the operating temperature of the OMT and directional coupler to 20 K, not only reduces the noise temperature added by the OMT and directional coupler themselves, but also further reduces the system noise temperature, compared to the receiver of [19].

Our OMT design consists of a very compact circular OMJ of length 1.26 λ_0 (at 1.55 GHz), and of two identical 180° hybrid power combiners, previously described in [20]. The proposed OMJ is based on the idea of the OMJ presented in [11], but it is designed and manufactured for low-temperature cooling, thus requiring to effectively handle the thermal gap between the antenna system, working at room temperature, and the cryogenic part of the receiver.

An early version of the circular OMJ presented in this paper was proposed in [21]. However, this conference paper describes only the Orthomode Junction, which, besides, was found not be effective for the required application. Actually, it was designed to operate at the cryogenic temperature of 80 K, whereas, in order to improve the performance of the radio astronomy receiver, we subsequently decided to further lower the OMT temperature of operation to 20 K. Moreover, in that paper, the characterization and test results of the full OMT are not given.

The proposed OMJ has been designed and optimized by using the commercial electromagnetic simulator CST Microwave Studio 2014. Then, the complete OMT (composed by the OMJ and two 180° hybrid power combiners) has been fabricated and tested, and a very good agreement is obtained between experimental results and predicted performance.

The OMT was experimentally tested at room temperature, while estimates of its performance at cryogenic temperatures are derived by accounting for the variation of the Ohmic losses, which reduce by lowering temperature with a well-predicted behaviour [22].

II. Architecture of the L-Band OMT

The sketch of the proposed L-band orthomode transducer is illustrated in Fig. 1a. This device consists of three distinct mechanical parts: *a)* a circular waveguide orthomode junction (see also Fig. 1b) with 4 coaxial outputs and *b)* two identical 180° hybrid power combiners based on a double ridged waveguide (DRWG) cavity [20] (see also Fig. 2 (a) and Fig. 2 (b)). Both the OMJ and the DRWG 180° hybrids are designed to reduce their physical dimension and weight in order to facilitate cooling at cryogenic temperature. In this paper we focus on design of the OMJ, since the DRWG hybrids have been thoroughly described in [20]. A different type of hybrid power combiner could be used, other than the DRWG configuration, as for example the dual-probe rectangular waveguide transition adopted in [11]. However, rescaling that configuration in the L-Band would require using WR650 waveguides, which have transverse dimension of 165.1 mm x 82.55 mm, whereas the DRWG hybrid transverse dimension is only 70 mm x 57.2 mm, thus reducing the transverse area of about one third. As apparent from Figs. 2 (a), 2 (b), and 3 (d), the transverse dimension of the DRWG hybrids has been optimized in order to minimize the diameter of the cryostat. More compact configurations, based on planar microstrip realization, could also be employed, but such a solution has been discarded, due to higher losses compared to waveguides.

The OMJ is a six electrical port device, with one physical circular waveguide input corresponding to the two orthogonal linearly polarized input channels, denoted in the following as electrical port 1 and port 2, and four output ports, denoted as ports 3, 4, 5, and 6 (see Fig. 1). This component has been realized with a circular waveguide with input diameter of D_1 = 172 mm, matched to the D_0 = 190 mm diameter of the L-Band feed through a conical waveguide transition (see Figs. 1 and 2). An annular metallic tuning stub is located at the base of the circular waveguide in order to match the RF signal from the L-band feed. The Signals from opposite output ports of the orthomode junction are then recombined by the DRWG 180° hybrids using four identical coaxial probes, which are symmetrically arranged inside the circular waveguide and located approximately one quarter wavelength from the circular waveguide backshort.

The L-band feed (and, as a consequence, the input port of the OMJ) operates at room temperature (300 K) within atmospheric pressure, whereas the other components of the receiver chain, including the two 180° hybrid power combiners, connected at the outputs of the OMJ with circular waveguide-coaxial transitions, are housed inside a vacuum-pumped cryostat and thermalized at 20 K in order to reduce their thermal noise.

The vacuum window that isolates the RF components located inside the vacuum-pumped cryostat (pressure below 10^{-4} mbar) from the feed at atmospheric pressure, consists of a 125µm thick Kapton® vacuum barrier (with dielectric permittivity 3.5 and tanδ = 0.001) which is sustained by a conically tapered section of Styrodur® 3035 CS (see Fig. 2 (c)). The Styrodur is housed inside a conically tapered metallic section between two circular waveguides, one at 300 K on the feed-horn side and the other on the cryogenic OMJ side. At L-band frequencies, the Styrodur is transparent to the incoming signal radiation because its dielectric constant is very close to 1 and its dielectric losses are negligible.

In other words, the OMJ input operates at 300 K, whereas the circular waveguide-coaxial transitions (i.e. the output coaxial probes) should operate at the cryogenic temperature of 20 K or below. Therefore, special care was taken in the OMJ design in order to insure the desired temperature gradient. This is obtained by using thermal gaps together with low thermal conductivity G10 (a fiberglass epoxy material) supports (discussed further down).

The temperature of 20 K is achieved using a two-stage cryo-refrigeration system. The maximum thermal power dissipation admitted at each stage must be within prescribed specifications of the two-stage cryo-cooler, which has a nominal temperature of 77 K on the first stage, and of 20 K on the second stage. No further details on the structure of the cryostat and on the refrigeration process are given, since this is beyond the scope of this paper. However, the desired physical temperatures are obtained when the heat power dissipation is less than 15 W on the first stage, and less than 3 W on the second stage. This is achieved by dividing the OMJ into three parts named “Stage 0” (at 300 K), “Stage 1” (at 77 K), and “Stage 2” (at 20 K) (see Fig. 2 (c)). These parts are separated by insulating air-gaps of thickness T = 0.5 mm. We have verified, by separate CST simulation, that such small air-gaps (T = 0.5 mm ≅ λ_g/500, being λ_g the guided wavelength at 1.55 GHz) introduce a very low insertion loss and low reflection. The simulated average insertion loss over the frequency band 1.3 GHz – 1.8 GHz, due to two air-gaps spaced L_1 = 49.5 mm in a 172 mm diameter circular waveguide, is less than 0.02 dB.

In this way, we obtain *a)* a conical waveguide transition, with diameters D_0 and D_1 and height L_0 = 85 mm, at 300 K, *b)* a circular waveguide with constant section of diameter D_1 and height L_1 = 49.5 mm embedded inside stage 1 at 77 K, and *c)* a circular waveguide-coaxial transition with height L_2 = 106.5 mm embedded inside stage 2 (at 20 K) of the cryostat.

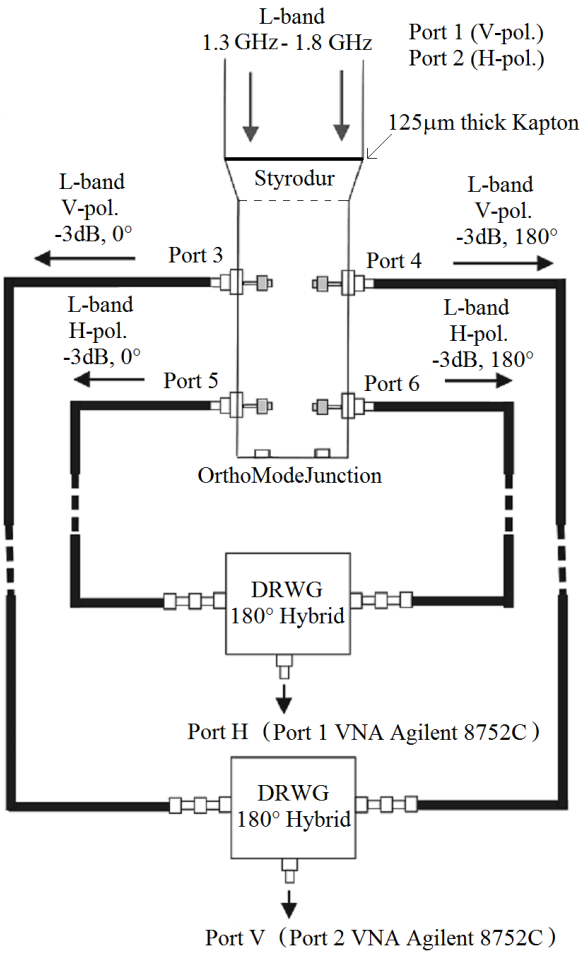

Fig. 1. (a) Sketch of the L-Band OMT showing the OrthoMode Junction, the two 180° hybrids and the interconnecting cables. The two couples of probes are symmetrically disposed inside the OMJ but are depicted at different distance in the OMJ cavity for drawing clarity; (b) Internal detail of the OrthoMode Junction, showing the real configuration of the probes.

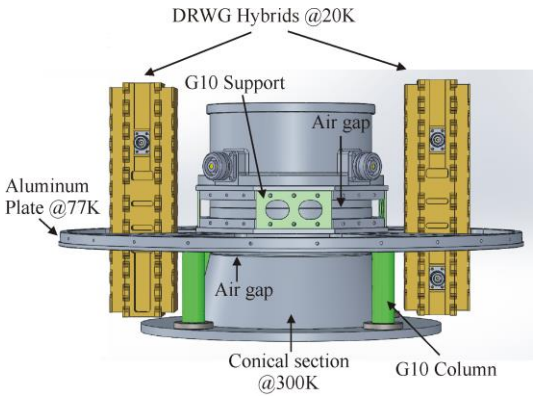

(a)

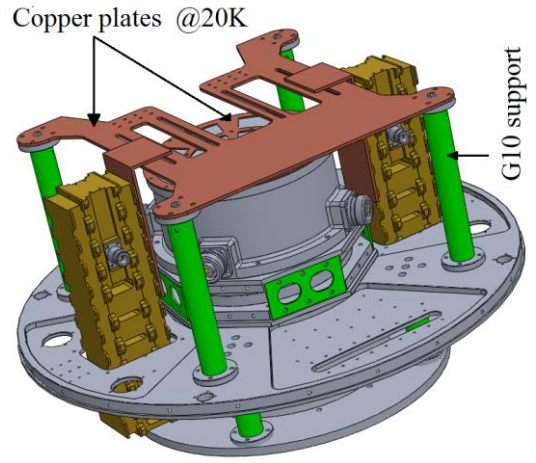

(b)

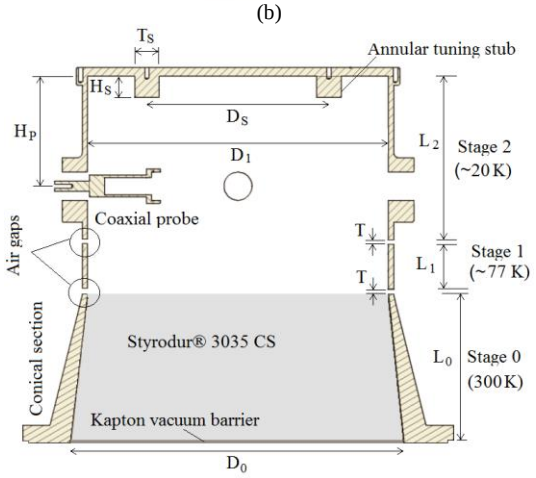

(c)

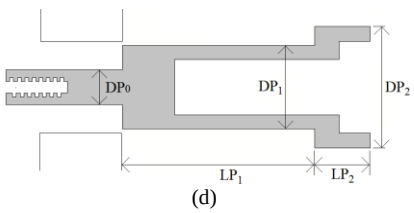

(d)

Fig. 2. (a) 3D view of the OMJ and DRWG 180° hybrids (supports for DRWG hybrids and coaxial cables between OMJ and hybrids are not shown); (b) 3D view of the OMJ and DRWG 180° hybrids: the DRWG Hybrids and the backshort of the OMJ are connected to copper plates @ 20K, the DRWG hybrids pass through holes in the aluminium plate at 77 K, without any contact with this plate; (c) cross-section of the OMJ; (d) detailed view of the OMJ coaxial probe.

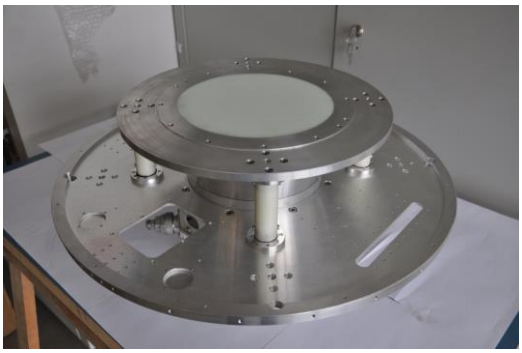

(a)

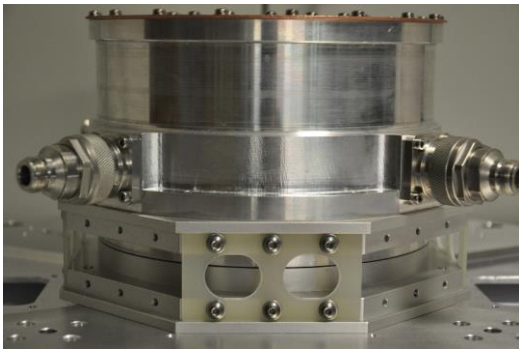

(b)

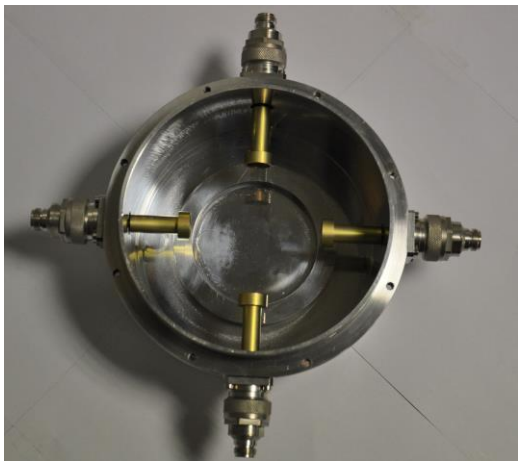

(c)

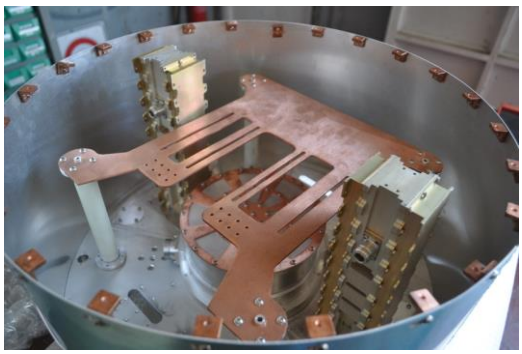

(d)

Fig. 3. Photos of fabricated OMJ prototype: (a) external view of the conical waveguide transition; (b) external view: detail of the circular waveguide section, circular waveguide-coaxial transitions, and air gap between stages 1 and 2; (c) internal view: detail of the coaxial probes; (d) internal view of the full orthomode transducer installed inside the cryostat.

Each air-gap between two metallic frames needs a support of insulating material with a thermal conductivity as low as possible to minimize the thermal flow. Four cylindrical columns of G10 material have been used to maintain the mechanical parts of stage 0 and stage 1 separated by a small air-gap (see Fig. 2 (a) and Fig. 3 (a)). As a support for the air-gap between stage 1 and stage 2 we have used four supports of G10 material (see Fig. 2 (a) and Fig. 3 (b)), each one modelled as a holed plate, designed and optimised to minimize the thermal flow [22, 23].

The design features undertaken and described above allow to limit the heat dissipation on the 1st and 2nd stages of the cryo-cooler to respectively 3.7 W (25% of the maximum admitted dissipation) and 2.5 W (85% of the maximum admitted dissipation). Such values have been obtained by estimating, through thermal simulations performed with the software Solidworks (version 2014) and through expressions derived by [22, 23], the thermal contribution of all the components inside the cryostat, and of the cryostat itself. The detailed analytical computation of the thermal load in the different parts of the cryogenic system is quite long and it is not reported here, since it is beyond the scope of this paper.

Figure 4 depicts the thermal analysis of the structure, and shows the effectiveness of the proposed design.

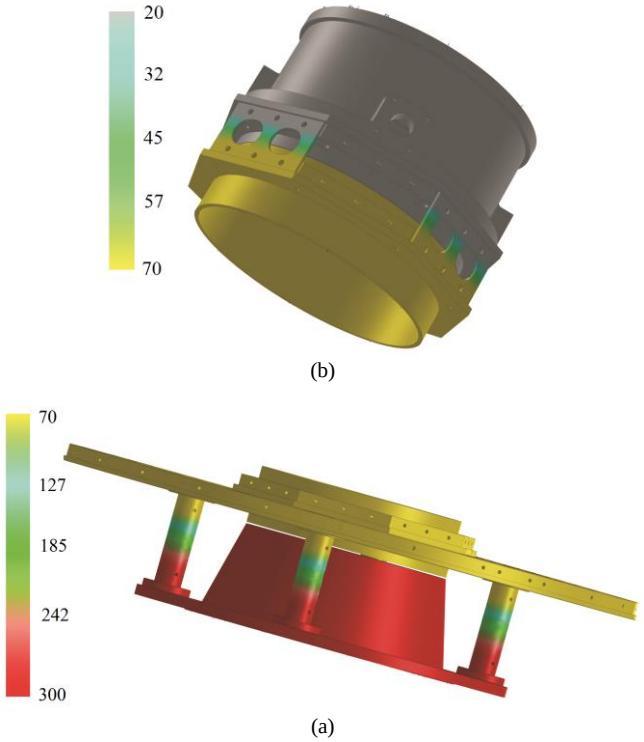

Fig. 4. Thermal analysis of the mechanical structure of the air-gap between stage 0 and stage 1 (bottom image), and of the air-gap between stage 1 and stage 2 (top image). A reference color scale for the temperature (in K) is shown on the left of each image.

As a result, on the 2nd stage of the cryostat, containing the circular waveguide-coaxial transition, we obtain a physical temperature of 17 K, within the prescribed goal.

III. Design and Test Results of the OMJ

The structure of the proposed orthomode junction shown in Fig. 2 (c) is very compact: if we exclude the output coaxial connectors and the input conical transition, the OMJ is a cylinder of height L_1+L_2+2T = 157 mm and diameter D_1 = 172 mm, which fills up only 0.27 liters of the cryostat volume.

The two orthogonal fundamental TE_{11} modes of the input circular waveguide, associated with the polarizations V and H of the RF input signal (see Fig. 1), propagate as independent linear polarizations when the frequency is beyond the waveguide cut-off value (f_c = 1.021 GHz). Then, the input signal is split (-3 dB) out-of-phase (180° phase difference) by pairs of opposite probes. The symmetry of the structure avoids the excitation of higher-order modes over the L-band (f_{cTM01} = 1.334 GHz and f_{cTE21} = 1.695 GHz). An annular tuning stub at the base of the OMJ circular waveguide (fixed-tuned backshort) allows achieving broadband operation with low input reflection coefficient.

The electromagnetic design and optimization of the OMJ has been performed by using CST Microwave Studio. The probes and the tuning stub have been designed and optimized to match the RF signal from the L-band feed, i.e. in order to match the 190 mm diameter circular waveguide ports (ports 1 and 2 in Fig. 1) of the OMJ. The position of the coaxial probes resulting in best performance is obtained for H_P = 62.5 mm from the backshort (see Fig. 2 (c)).

Each probe (see Fig. 2 (d)) consists of three coaxial cylinders of different diameter with the smaller section which is screwed to the pin of a commercial 50 Ω 7/16-type connector, and has, therefore, the same diameter DP_0 = 5.4 mm. LP_1 and LP_2 are fixed to 32 mm and 8 mm respectively, with the constraint that $LP_1 + LP_2 \leq 40$ mm, in order to reduce mechanical vibrations which could limit the amplitude stability of the receiver, whereas DP_1 and DP_2 have been selected as design parameters.

The geometrical parameters of the annular tuning stub are shown in Fig. 2 (c). The diameter D_S is fixed to $0.5D_1$ = 86 mm and the height H_S has been fixed to 10 mm. Then, the width T_S is selected as a further matching parameter.

After the CST optimization, we obtain DP_1 = 12.4 mm, DP_2 = 19.6 mm, and T_S = 35 mm.

The designed OMJ was assembled in the laboratories of the INAF (National institute for astrophysics)-Astronomical Observatory of Cagliari, and then measured at room temperature using a commercial two-port HP8720C Vector Network Analyzer (VNA).

In order to calibrate the VNA and measure the return loss, the transmission, and the cross-polarization of the OMJ, we have designed and fabricated two identical coaxial-to-circular-waveguide transitions. Each transition consists of two blocks, a rectangular-to-circular transition and a coaxial-to-rectangular transition. The first block is a circular waveguide with diameter of 190 mm that attaches to the OMJ, cascaded with a square waveguide and a linearly tapered square to rectangular waveguide (see Fig. 5). The other block is a coaxial probe, which extracts the signal from a WR650 waveguide (see Fig. 6). In order to improve the accuracy of the measurement, the VNA has been calibrated using the TRL procedure [24] to

remove the effect of the coaxial to circular waveguide transition.

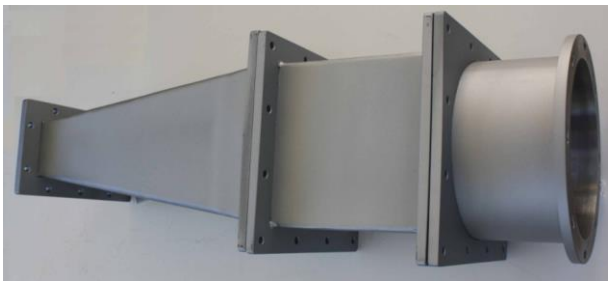

Fig. 5. Photo of the rectangular-to-circular waveguide transition consisting of three aligned mechanical parts. The flange on the rectangular side allows connection to the coaxial to rectangular transition. The flange on the circular side allows connection to the OMJ.

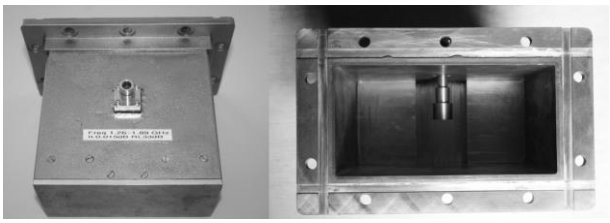

Fig. 6. Photos of the WR650 rectangular-to-coaxial waveguide transition. The left panel shows the N-type coaxial cable output connector. The right panel shows an internal view of the transition.

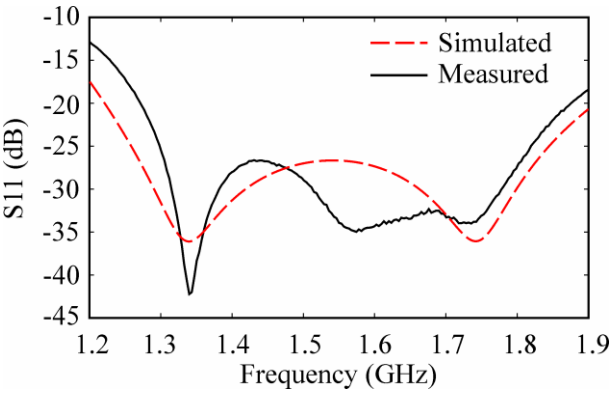

Fig. 7. Simulated and measured reflection coefficient (S_{11}) of the OMJ designed for operation across 1.3-1.8 GHz.

Figure 7 shows the simulated and measured input reflection $|S_{11}|$ of the OMJ. A good match is obtained between prediction and experiment, with the simulated $|S_{11}|$ less than -27 dB and the measured one less than -25 dB over the operating frequencies (1.3 GHz - 1.8 GHz).

Figure 8 shows the simulated and measured amplitude of the transmission coefficient (S_{31}) for the V-polarization: the transmissions between the input port and each of the two symmetric output coaxial ports is very close to the expected value of -3 dB, with a very good agreement between simulation and measurement. The simulated amplitude of S_{41} is identical to the amplitude of S_{31} due to the symmetry of the component, and the agreement with experimental data is the same as observed for S_{31}. Moreover, the signals at the two symmetric coaxial outputs (ports 3 and 4) are around 180° out of phase at all frequencies of interest (see the dashed-dotted line in Fig. 8), with a very small discrepancy around 0.15°. Only simulated results are provided for this phase difference because the experimental setup would require two independent and consecutive measurements of the phases of S_{31} and S_{41} using the available two-port VNA. This would require moving one cable of the VNA from port 3 to port 4 (or vice versa) of the OMJ, which modifies the cable phase and invalidates the calibration parameters, thus resulting in a large measurement error.

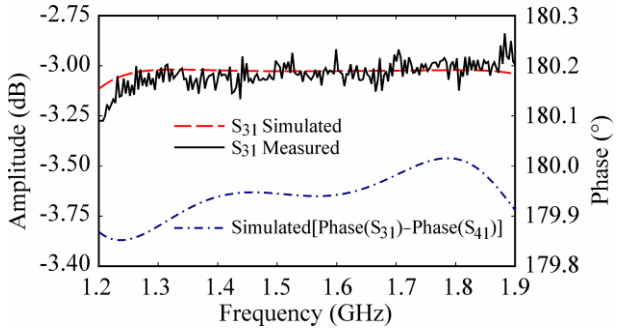

Fig. 8. Amplitude of the transmission coefficient S_{31} and simulated phase difference between the outputs at ports 3 and 4.

Due to the symmetry of the OMJ, similar results for the S-parameter are expected for the V-polarization and for the H-polarization.

The simulated cross-polarization of the perfectly symmetric OMJ is about -70 dB (scattering parameters S_{51} or S_{23}), and it is set by numerical rounding off errors, whereas the measured cross-polarization is below -45dB over the frequency band (see Fig. 9).

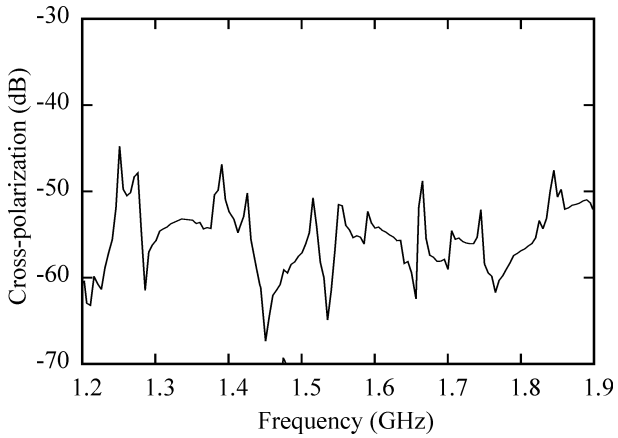

Fig. 9. Measured cross-polarization (S_{51}) of the OMJ.

IV. Experimental Results of the Fully Assembled OMT

The OMT (see Fig. 1, Fig. 2 (a), Fig. 2 (b), and Fig. 3 (d)) was fully assembled by connecting the four OMJ outputs to two identical 180° hybrid power combiners (see [20]) through equiphase 0.141″ copper semi-rigid coaxial cables with physical length 350 mm. The whole structure has been tested at room temperature using the HP8720C Vector Network Analyzer (see Fig. 1 and Fig. 10).

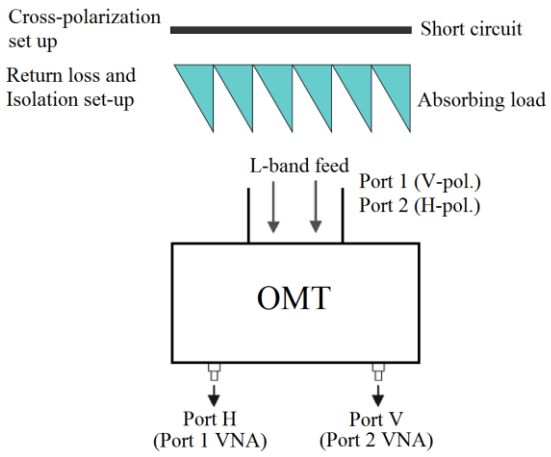

(a)

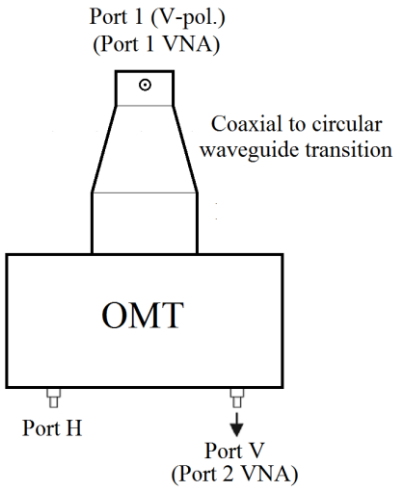

(b)

Fig. 10. Sketch of the OMT measurement set-up: (a) measurement set-up for cross-polarization, return loss at ports V and H, and isolation; (b) measurement set-up for input reflection and insertion loss.

The OMT has been characterized for some of its most important parameters: the reflection at the input port, the insertion loss, the reflection at the output ports (ports H and V in Fig. 1 and Fig. 10 (a)), the isolation, and the cross-polarization level. Different measurement set-up and calibrations of the VNA are required.

In the measurement set-up for return loss at the output ports, isolation and cross-polarization (see Fig. 10 (a)), which will be described in detail further down, the VNA has been calibrated at the N-type connector ports of the hybrids in order to remove the effects of the coaxial cables. On the other hand, the measurement set-up for reflection at the input port and insertion loss exploits the coaxial to circular waveguide transition shown in Figs. 5 and 6 to connect the OMT port 1 (V-pol) to VNA port 1, whereas port V of the OMT is connected to VNA port 2 (see Fig. 10 (b)). In this case, port 1 of the VNA has been calibrated using the TLR procedure to remove the effect of the coaxial to circular waveguide transition, whereas port 2 of the VNA has been calibrated at the N-type connector port of the hybrid.

An open circular waveguide with diameter D_0 = 190 mm is quite well matched to free open space over the frequency band, resulting in a reflection coefficient below -25 dB (the reflection increases with decreasing frequency, this value being obtained at the lower frequency edge of the band of interest, i.e. 1.3 GHz). Thus, the reflection coefficients from the coaxial outputs of the OMT have been measured by terminating its circular waveguide input with an absorbing load placed in front of the circular waveguide, and then connecting the OMT outputs to the VNA coaxial ports (see Fig. 10 (a), Return Loss set-up). The simulated and measured reflection coefficients for the two linear polarization channels (S_{HH} and S_{VV}) are shown in Fig. 11. The measured reflection coefficients are less than -20 dB over the frequency band and are similar, in overall level, to simulated values, computed by cascading the scattering matrices of the simulated OMJ and simulated DRWG connected through coaxial 50 Ω lines.

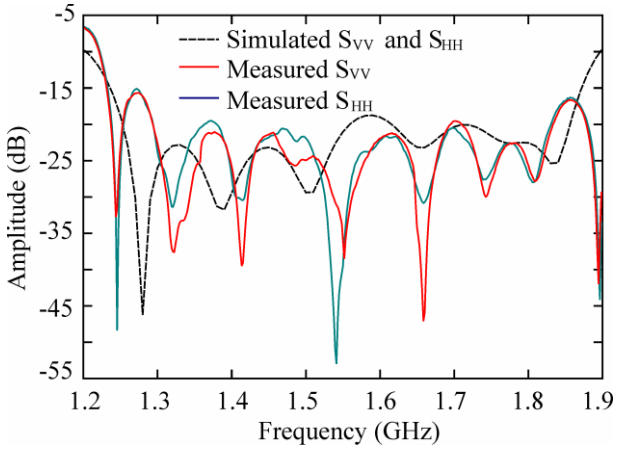

Fig. 11. Measured and simulated output reflection of the full OMT with the input circular waveguide terminated with an absorbing load.

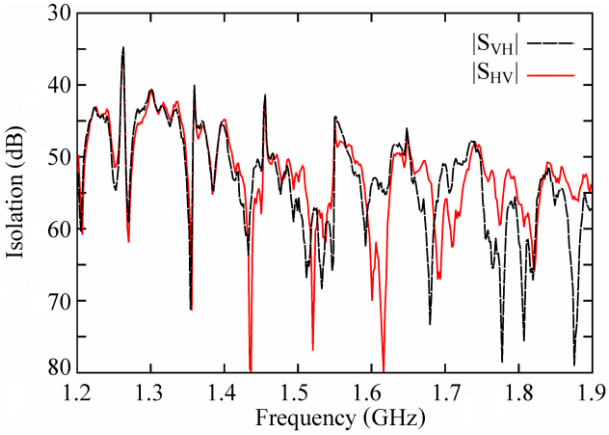

Fig. 12. Measured Isolation of the full OMT with the input circular waveguide terminated with an absorbing load.

An estimate of the OMT isolation has been obtained by measuring the transmission between the OMT output ports (i.e. S_{VH} and S_{HV}) when its circular waveguide input port is terminated with the absorbing load (see Fig. 10 (a), Isolation

set-up). As shown in Fig. 12, the measured OMT isolation is more than 40 dB over the frequency band.

The cross-polarization of the OMT has been estimated by measuring the transmission from one of the OMT coaxial output to the other coaxial output, with the input circular waveguide terminated into a short circuit, which has been realized with an aluminum plate (see Fig. 10a, Cross-Polarization set-up). The measured cross polarization level of the OMT is below -35 dB over the band of interest, as shown in Fig. 13. The degradation of the cross-polarization level of the complete OMT with respect to the measured cross-polarization of the OMJ (which is -45 dB), is mainly due to the deviation from the ideal coupling and 180° phase difference of the DRWG hybrids, which is respectively ± 0.25 dB and ± 0.9° [20].

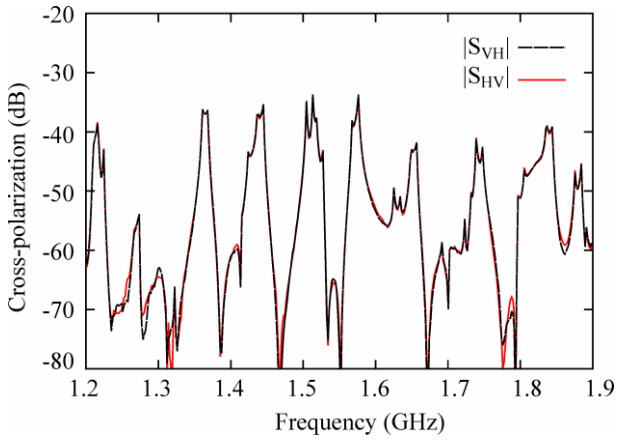

Fig. 13. Measured cross-polarization of the OMT with the input circular waveguide terminated with a short circuit load.

The reflection at the input port and the insertion loss of the OMT are measured using the set-up of Fig. 10 (b). In Fig. 14 the reflection coefficient is reported. A good input match is achieved, with $|S_{11}|$ less than -18 dB between 1.3 GHz and 1.8 GHz. In Fig. 15 the insertion loss is depicted, showing an average value of about 0.48 dB over the frequency band. The thermal noise contribution due to the insertion loss of such component at 300 K would account for about 35 K and is expected to reduce with physical temperature.

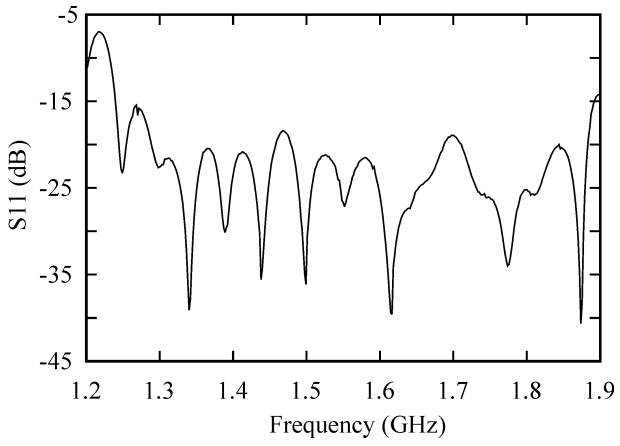

Fig. 14. Measured reflection coefficient (S_{11}) of the OMT.

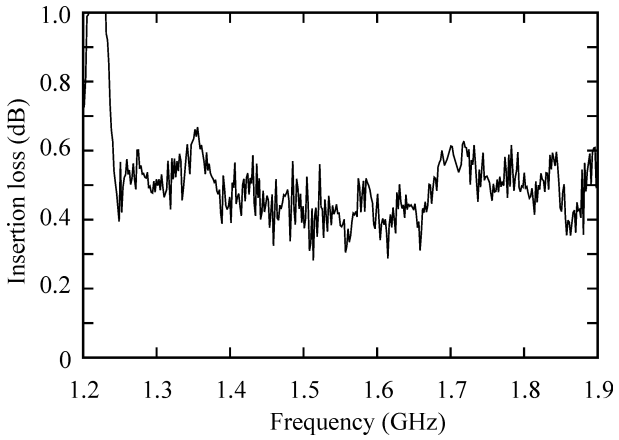

Fig. 15. Measured insertion loss of the OMT at 300 K.

Although the OMT characterization has been done at room temperature, the DRWG hybrids have been tested both at room temperature and at the cryogenic temperature of 77 K. Measurements of the hybrids at 20 K have not been carried out. The copper semi-rigid coaxial cables have been tested at room temperature; measurements at the cryogenic temperatures of 77 K and 20 K are available from [25].

Fig. 16 shows the insertion loss of the DRWG hybrids at 300 K and 77 K, whereas Fig. 17 plots the insertion loss of the copper semi-rigid coaxial cables at 300 K, 77 K, and 20 K. The noise temperature added by the DRWG hybrids is estimated to be about 10.5 K at 300 K (average insertion loss around 0.15 dB between 1.3 GHz and 1.8 GHz), and 0.9 K at 77K (average insertion loss around 0.05 dB), whereas the noise temperature added by the copper semi-rigid coaxial cables is about 10.5 K at 300 K (average insertion loss = 0.15 dB), 1.2 K at 77 K (average insertion loss = 0.07 dB), and 0.2 K at 20 K (average insertion loss = 0.04 dB).

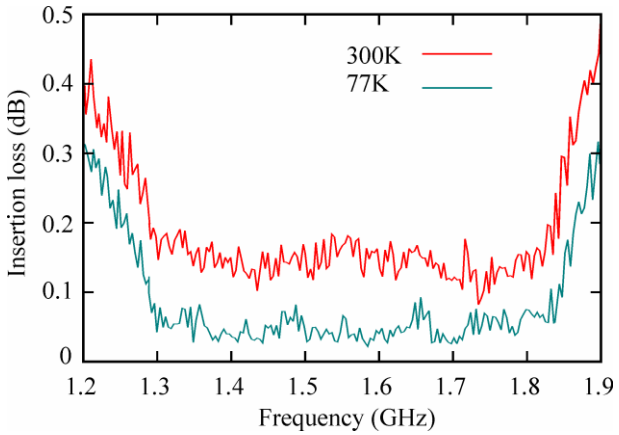

Fig. 16. Measured insertion loss of the DRWG Hybrid.

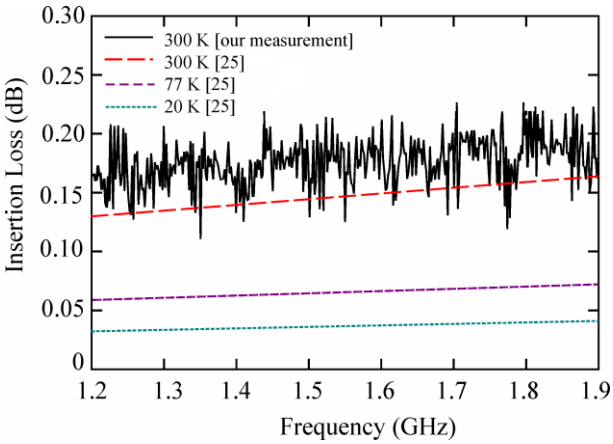

Fig. 17. Measured Insertion Loss of copper semi-rigid coaxial cables of length 350 mm at different temperatures.

The results of the thermal analysis of the DRWG hybrids and coaxial cables suggest a significant reduction of the insertion loss of the full OMT at cryogenic temperatures, compared to its value at 300 K. The noise temperature added by the OMT cooled at 77 K is expected to be less than 5.5 K, since its insertion loss is expected to be less than 0.3 dB (estimate based on the insertion loss of DRWG hybrids and coaxial cables at 77 K). On the other hand, the noise temperature added by the OMT at 20 K is expected to be less than 1.3 K (OMT insertion loss expected to be less than 0.27 dB). The latter value is a significant overestimate because we are considering only the insertion loss reduction (from 300 K to 20 K) due to the copper semi-rigid coaxial cables (hybrids and OMJ are not tested at 20 K).

The reduction of the noise temperature upon cooling at 20 K is significant for the complete OMT, which justify our design effort.

V. Conclusion

We have presented the design, construction and test of a compact L-Band (1.3 GHz - 1.8 GHz) OMT based on three separate mechanical parts which are connected through commercial coaxial cables: an orthomode junction in circular waveguide, presented in this work, and two hybrid power combiners in double ridged waveguide, proposed in a previous work by the same authors. The OMT is intended to be used in the L-Band receiver of the Sardinia Radio Telescope, which operates at the cryogenic temperature of 20 K in order to reduce the thermal noise of the receiving chain. The proposed component has a very compact structure, as required by the constraints of the refrigeration process, and provides high performance over the operating frequency band. A very good agreement is observed between measurement and predicted performance, with isolation of 40 dB, cross polarization of -35 dB, average insertion loss at room temperature of about 0.48 dB over the operating bandwidth, and an estimated noise temperature added by the component less than 1.3 K at the cryogenic temperature of 20 K.

Acknowledgment

The authors would like to thank Pasqualino Marongiu at INAF - Astronomical Observatory of Cagliari for the design of mechanical blocks.

References

[1] A. M. Bøifot, "Classification of Ortho-mode transducers," *European Transactions on Telecommunications*, vol. 2, no. 5, pp. 503–510, September/October 1991.

[2] R. Ambrosini, et al., "Commissioning of the Sardinia Radio Telescope in Italy: Results and perspectives," *General Assembly and Scientific Symposium (URSI GASS), 2014 XXXIth URSI*, 16-23 August 2013.

[3] G. Valente, G. Montisci, and S. Mariotti, "High-performance microstrip directional coupler for radio-astronomical receivers at cryogenic temperature," *Electronics Letters*, vol. 50, pp. 449-451, Mar. 2014.

[4] A. M. Bøifot, E. Lier, T. Schaug-Pettersen, "Simple and broadband orthomode transducer," *IEE Proceedings*, vol. 137, pt. H, No. 6, pp. 396-400, Dec. 1990.

[5] M. A. Meyer and H. B. Goldberg, "Applications of the turnstile junction," *IRE Trans. Microw. Theory Tech.*., vol. MTT-3, no. 6, pp. 40-45, 1955.

[6] A. Navarrini and R. L. Plambeck, "A turnstile junction waveguide orthomode transducer," *IEEE Trans. Microw. Theory Techn.*, vol. 54, no. 1, pp. 272-277, 2006.

[7] A. Navarrini, A. Bolatto, and R. L. Plambeck, "Test of 1 mm Band Turnstile Junction Waveguide Orthomode Transducer," *17th International Symp. on Space Terahertz Tech.*, pp. 99-102, Paris, France, May 10-12, 2006.

[8] G. Pisano et al., "A broadband WR10 turnstile junction orthomode transducer," *IEEE Microw. Compon. Lett.*, vol. 17, no. 4, pp. 286–288, Apr. 2007.

[9] J. H. Hwang, Y. Oh, "Compact Orthomode Transducer Using Single-Ridged Triangular Waveguides," *IEEE Microw. Compon. Lett.*, vol. 21, no. 8, August 2011.

[10] G. M. Coutts, "Octave Bandwidth Orthomode Transducers for the Expanded Very Large Array," *IEEE Trans. Antennas Propag.*, vol. 59, no. 6, June 2011.

[11] G. Engargiola and A. Navarrini, "K-Band Orthomode Transducer With Waveguide Ports and Balanced Coaxial Probes," *IEEE Trans. Microw. Theory Techn.*, vol. 53, no. 5, May 2005.

[12] D. Bock, "Measurements of a scale-model ortho-mode transducer," BIMA memo 74, July 7, 1999.

[13] R. W. Jackson, "A planar orthomode transducer," *IEEE Microw. Compon. Lett.*, Vol. 11, Issue 12, pp. 483 -485, Dec. 2001.

[14] G. Engargiola and R. L. Plambeck, "Tests of a planar L-band orthomode transducer in circular waveguide," *Rev. Scientific Instruments*, Vol. 74, No. 3, March 2003.

[15] P. K. Grimes, O.G. King, G. Yassin, and M.E. Jones, "Compact broadband planar orthomode transducer," *Electronics Letters*, Vol. 43, Issue 21, pp 1146-1147, Oct. 2007.

[16] M. A. Morgan, J. R. Fisher, and T. A. Boyd, "Compact Orthomode Transducers Using Digital Polarization Synthesis," *IEEE Trans. Microw. Theory Techn.*, vol. 58, no. 12, pp. 3666-3676, Dec. 2010.

[17] R. Lehmensiek and I. P. Theron, "L-band feed horn and orthogonal mode transducer for the KAT-7 radio telescope," *IEEE Trans. Antennas Propag.*, vol. 59, no. 6, pp. 1894-1901, Jun. 2011.

[18] R. Lehmensiek and I. P. Theron, "Compact low loss L-band orthomode transducer," *Proc. Int. Conf. Electromagn. Adv. Appl. (ICEAA)*, Sydney, Australia, Sep. 2010, pp. 228-231.

[19] R. Lehmensiek and I. P. Theron, "Minimizing the MeerKAT system noise temperature," *31th URSI General Assembly and Scientific Symposium (GASS)*, Beijing, China, Aug. 2014, pp. 1-4.

[20] G. Valente, A. Navarrini, and T. Pisanu, "Double Ridged 180° Hybrid Power Divider with Integrated Band Pass Filter," *IEEE Microw. Compon. Lett.*, vol. 21, no. 1, pp. 13-15, Jan. 2011.

[21] T. Pisanu, P. Marongiu, A. Navarrini, and G. Valente, "A compact L-band Ortho Mode Junction," *Proc. SPIE 7741, Millimeter, Submillimeter, and Far-Infrared Detectors and Instrumentation for Astronomy V*, 774124 (15 July 2010), 10 pages.

[22] J. G. Weisend II, *Handbook of Cryogenic Engineering*, Philadelphia: Taylor & Francis, 1998.
[23] NIST Cryogenics Technologies Group. Available: http://cryogenics.nist.gov/MPropsMAY/materialproperties.htm
[24] J. Curran, "TRL Calibration for Non-Coaxial Measurements", Semiconductor Test Symposium, Hewlett-Packard Company. Available: http://www.hparchive.com/seminar_notes/a-215.pdf
[25] S. Weinreb: "Cryogenic performance of microwave terminations, attenuators, absorbers, and coaxial cable," National Radio Astronomy Observatory, Charlottesville, Virginia, Electronics division internal report no. 223, 1982.